

1 **Preconditioning and triggering of offshore slope failures and turbidity currents**  
2 **revealed by most detailed monitoring yet at a fjord-head delta**

3 Clare, M.A.<sup>1\*</sup>, Hughes Clarke, J.E.<sup>2</sup>, Talling, P.J.<sup>1</sup>, Cartigny, M.J.<sup>1</sup>, Pratomo, D.G.<sup>3</sup>

4 <sup>1</sup>National Oceanography Centre Southampton, European Way, Southampton,  
5 Hampshire, SO14 3ZH

6 <sup>2</sup>Center for Coastal and Ocean Mapping, University of New Hampshire, USA

7 <sup>3</sup>Ocean Mapping Group, University of New Brunswick, Canada

8 \*email: [michael.clare@noc.ac.uk](mailto:michael.clare@noc.ac.uk)

9 **Key Points:**

- 10 • Detailed monitoring of landslides and turbidity currents at fjord-head delta
- 11 • 106 mass movements recorded enabling statistical analysis for the first time
- 12 • Elevated river discharge leads to delayed slope failure, not hyperpycnal flow
- 13 • Most significant control on turbidity current timing is delta-top bed shear stress
- 14 • River discharge and low tides increased flux of bedload driven over the delta lip

15

16 **Key words**

17 River delta, submarine landslides, turbidity current, geohazard, mass failure, sediment  
18 flow

19 **ABSTRACT**

20 Rivers and turbidity currents are the two most important sediment transport processes  
21 by volume on Earth. Various hypotheses have been proposed for triggering of turbidity

22 currents offshore from river mouths, including direct plunging of river discharge, delta  
23 mouth bar flushing or slope failure caused by low tides and gas expansion, earthquakes  
24 and rapid sedimentation. During 2011, 106 turbidity currents were monitored at  
25 Squamish Delta, British Columbia. This enables statistical analysis of timing, frequency  
26 and triggers. The largest peaks in river discharge did not create hyperpycnal flows.  
27 Instead, delayed delta-lip failures occurred 8-11 hours after flood peaks, due to  
28 cumulative delta top sedimentation and tidally-induced pore pressure changes. Elevated  
29 river discharge is thus a significant control on the timing and rate of turbidity currents  
30 but not directly due to plunging river water. Elevated river discharge and focussing of  
31 river discharge at low tides cause increased sediment transport across the delta-lip,  
32 which is the most significant of all controls on flow timing in this setting.

### 33 **1. Introduction**

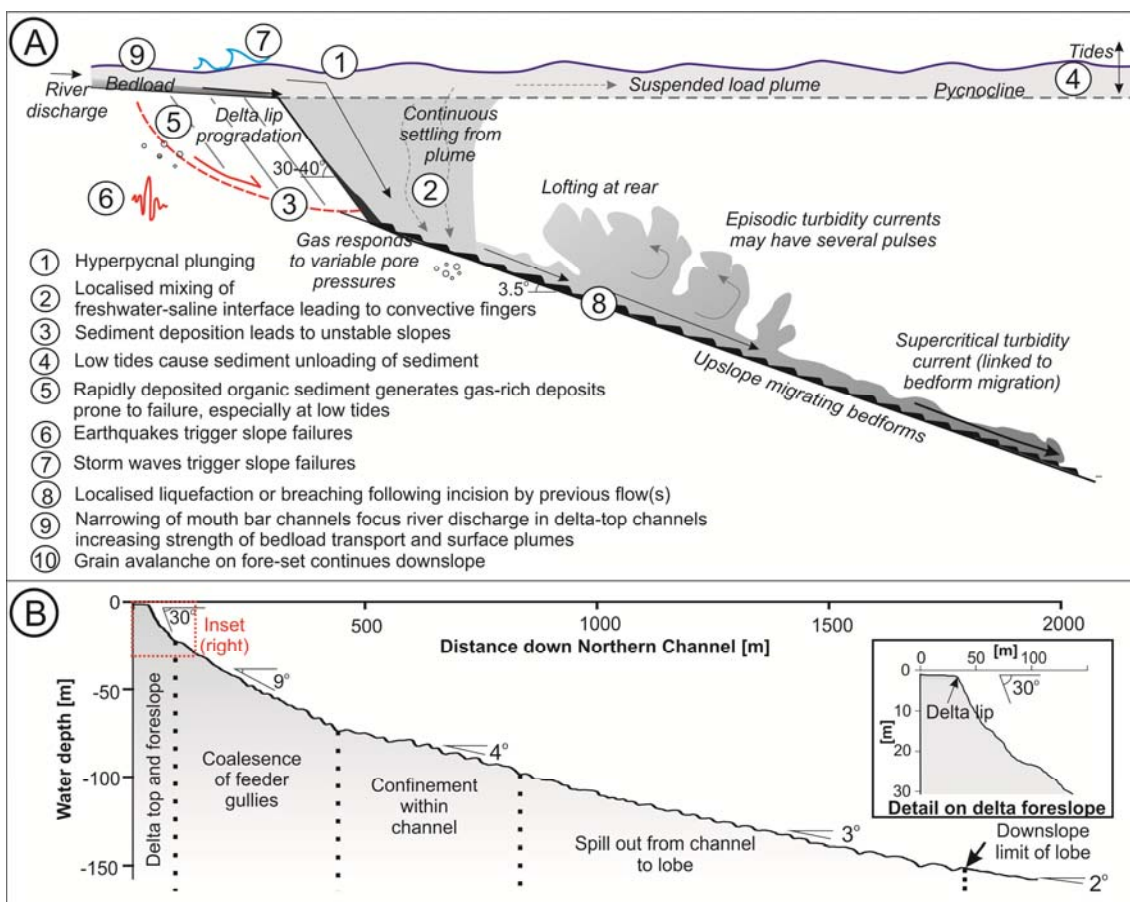
34 Rivers and offshore turbidity currents are the two most volumetrically important  
35 sediment transport processes on Earth, and form its most extensive sedimentary deposits  
36 (Ingersoll et al., 2003). It is important to understand how these two types of sediment-  
37 and-water flows are linked. For instance, how do changes in discharge from a river  
38 affect the frequency and character of turbidity currents, and how exactly are turbidity  
39 currents triggered immediately offshore from river mouths? Understanding controls on  
40 turbidity current frequency is also societally important as turbidity currents damage  
41 important seafloor infrastructure including telecommunications cables or pipelines  
42 (Carter et al., 2014), whilst submarine slope failures can trigger tsunamis (e.g. Prior et  
43 al., 1982).

44 River deltas can be sub-divided according factors that include the degree of wave or  
45 tidal action, magnitude and type of river (e.g. bedload or suspended load-dominated;

46 sand or gravel), offshore gradient, development of mouth bars and inertial or frictional  
47 mouth jets, and whether the river enters seawater or freshwater  
48 (Wright, 1977; Orton and Reading, 1993). Here we study  
49 offshore slope failure and turbidity currents generated at a marine fjord-head delta,  
50 which is one of the most common type of delta system globally. Fjord-head deltas are  
51 often characterised by limited fetch and hence wave heights, relatively steep offshore  
52 gradients, and coarse grained (sand or gravel) rivers with significant bedload transport  
53 from surrounding mountainous catchments. As with many other fjord head systems (e.g.  
54 Syvitski and Shaw, 1995), the delta that we study here is also affected by significant  
55 tides.

56 Multiple triggers are proposed for turbidity currents and landslides offshore from river  
57 mouths, including fjord-head systems (Figure 1; Forel, 1888; Mulder et al., 2003; Piper  
58 and Normark, 2009). Debate surrounds the relative importance of these different  
59 triggers in river-fed systems, and there is a compelling need to test these alternative  
60 hypotheses (Figure 1; Table 2). These preconditioning and triggering factors can be  
61 grouped into those due to plunging (hyperpycnal) river discharges that continue along  
62 the seafloor as turbidity currents, settling of sediment from a lower concentration  
63 surface (homopycnal) plume that generated underflows along the bed, or submerged  
64 slope failures that disintegrate to form turbidity currents. If sediment-laden river-water  
65 is dense enough to plunge, it continues to form a hyperpycnal turbidity current (Forel,  
66 1888; Mulder and Syvitski, 1995; Parsons et al., 2001; Mulder et al., 2003; label 1 in  
67 Figure 1). Mixing of the freshwater-saline interface can cause enhanced settling of  
68 sediment due to convective fingers, at much lower ( $>1 \text{ kg/m}^3$ ) sediment concentrations  
69 (2; Parsons et al., 2001). As river flow expands at the coast, rapid sediment deposition  
70 can create unstable slopes prone to failure, resulting in turbidity currents (3, Prior et al.,

71 1987; Carter et al., 2014). It has been proposed that slope failures can result from high  
 72 excess pore pressures due to such rapid sedimentation, tidal unloading of sediments (4)  
 73 and expansion of gas bubbles within organic rich deltaic sediment (5; Christian et al.,  
 74 1997), earthquake shaking (6; Carter et al., 2014), or cyclic loading by storm waves (7;  
 75 Prior et al., 1989). An initial turbidity current may cause failure by undercutting slopes,  
 76 and contraction of sediment may create prolonged failures called breaches (8; Van Den  
 77 Berg et al., 2002; Mastbergen and Van Den Berg, 2003). Low tides may also focus river  
 78 discharge in delta-top channels thereby increasing significantly the strength of bedload  
 79 transport and surface plumes (9; Prior et al., 1987; Hughes Clarke et al., 2012a). In areas  
 80 of steep offshore topography, avalanching of sediment across the delta-lip may generate  
 81 steep (30°) foresets that characterise Gilbert-type deltas (10; Gilbert, 1885; Postma et  
 82 al., 1988).



83

84 **Figure 1: (A) Previous hypotheses for triggering of slope failures and turbidity**  
85 **currents at fjord-head deltas with bedload-dominated rivers (upper panel; also see**  
86 **Table 2). (B) Water depth and slope angles based on Squamish delta slope (lower**  
87 **panel).**

88

89 However, these hypotheses are problematic to test as very few field data sets document  
90 the exact timing of turbidity currents and submerged slope failures, as they are difficult  
91 to monitor directly (Talling et al., 2015). Such information is key for determining the  
92 relative importance of river discharge, tides, or other triggering factors. No previous  
93 direct monitoring study has documented more than a few tens of turbidity currents; and  
94 in most cases far fewer (e.g. Prior et al., 1987 at Bute Inlet; Lambert and Giovanoli,  
95 1988 in Lake Geneva; Cooper et al., 2013 in Congo Canyon; Carter et al., 2014 in  
96 Gaoping Canyon; Xu et al., 2014 in Monterey Canyon). Statistical analysis of event  
97 frequency and triggers has therefore been restricted to much less precisely dated ancient  
98 turbidity current and landslide events, with comparisons only possible with longer-term  
99 processes such as sea level change (e.g. Droxler and Schlager, 1985;  
100 Clare et al., 2014).

101 Here we present the first statistical analysis of >100 precisely-timed individual  
102 submarine landslide and turbidity current events from Squamish Delta in British  
103 Columbia, Canada (Hughes Clarke et al., 2012a, 2014). Event timing was determined  
104 from (i) a seafloor Acoustic Doppler Current Profiler (ADCP), and (ii) 93  
105 approximately-daily repeat multibeam echo-sounder (MBES) surveys that document  
106 changes in seafloor morphology. This location represents arguably the most detailed  
107 monitoring of a turbidity current system that combines an exceptional number of repeat

108 mapping surveys with direct flow measurements (Hughes Clarke et al., 2011, 2012a,b;  
109 2014; Hughes Clarke, 2016).

110 Three distinct types of event are recorded in this dataset (Hughes Clarke et al., 2012a,  
111 2014). Infrequent, large-scale, deep-seated collapses of the prograding delta-lip are  
112 termed “delta-lip failures” More frequent events involve the upstream-migration of  
113 bedforms within channels on the submarine prodelta are termed “bedform events”.  
114 These bedform events may be further subdivided into those associated with an initial  
115 slope failure scar, and those that lack a visible (< 0.5-1 m high) failure scar (“events  
116 without a headscar”).

## 117 **2. Aims**

118 Our overall aim is to understand the factors that precondition or trigger slope failure and  
119 turbidity currents on this fjord-head delta using an exceptionally detailed field data set.  
120 The first specific aim is to understand the factors that cause large-scale (>20,000 m<sup>3</sup>)  
121 failures of the delta-lip, whilst the second aim is to understand the causes of bedform  
122 events. In the case of the second aim this includes statistical analysis of their  
123 relationship between the timing of these events and changes in river discharge and tidal  
124 elevation. Is river discharge or tidal elevation a stronger control, and do these two  
125 factors have independent or combined effects on turbidity current frequency? The  
126 implications of these associations are then discussed for understanding the physical  
127 mechanisms that trigger these flows.

128 **3. Methods**

129 **3.1. Squamish delta: An outstanding natural laboratory**

130 The Squamish River transports more than one million cubic metres of sediment per year  
131 to its delta and flows into Howe Sound (Figure 2A; Hickin, 1989). The river is heavily  
132 influenced by seasonal meltwater, as the winter discharge of  $\sim 100 \text{ m}^3/\text{s}$  increases in the  
133 freshet to  $>500 \text{ m}^3/\text{s}$ , with peaks of up to  $1,000 \text{ m}^3/\text{s}$  in summer. While enhanced  
134 suspended sediment occurs within the river plume during such discharge peaks, the  
135 values measured at more typical discharges (up to  $0.4 \text{ kg}/\text{m}^3$ ) are much lower than that  
136 required to overcome the density surfeit ( $0.7 \text{ kg}/\text{m}^3$ ) for plunging river water (Hughes  
137 Clarke et al., 2014). Spring tidal range may reach 5 m whereas neap tides have a range  
138 of  $\sim 3$  m. At low-water spring-tides, the river discharge is focused within a sub-tidal  
139 channel of 1 m depth and 200 m width where it reaches the delta-lip (Figure 2B&F).  
140 This delta-top channel is flanked by two intertidal sand flats, and comprises dominantly  
141 sandy-gravel deposits with a mean grain size of  $\sim 0.5$  to  $0.8$  mm. Seaward of the delta-  
142 lip, three main channels are found on the prodelta slope, termed “northern”, “central”  
143 and “southern” channels. At a distance of 2 km from the delta-lip, these channels open  
144 out and flows become unconfined (Figure 2C).

145

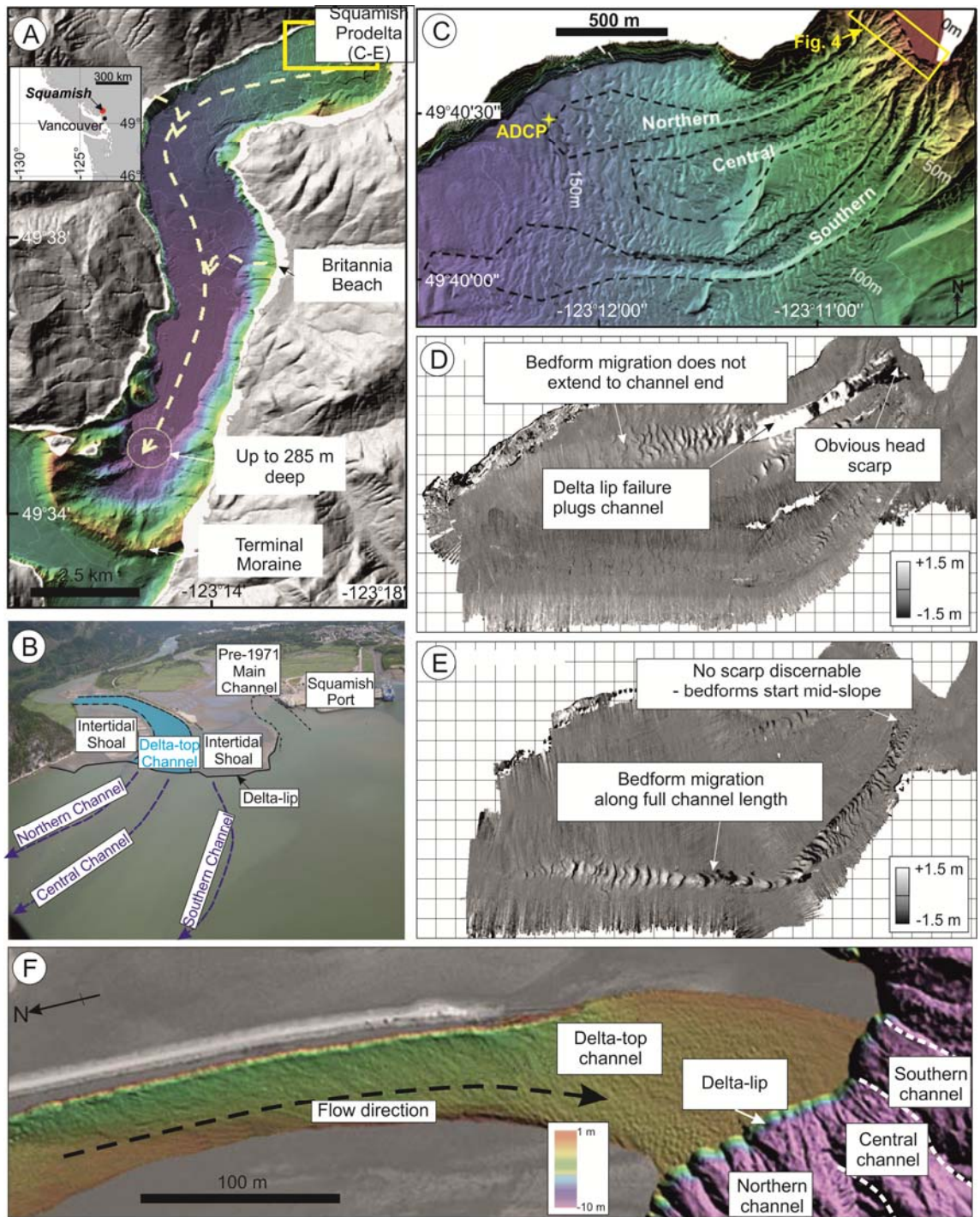
146 **3.2 Bathymetric changes related to landslide and turbidity current activity**

147 Squamish Delta is exceptionally well monitored as numerous multibeam surveys have  
148 been collected over eight years. 93 repeat surveys performed in 2011 enable the  
149 production of difference maps to observe daily change during the freshet. Changes in  
150 seafloor morphology have been shown to be related to slope failures and turbidity

151 currents (Hughes Clarke et al., 2012a,b, 2014). Water column imaging above bedforms  
152 in the prodelta channels has clearly imaged active turbidity currents that locally erode  
153 and deposit sediment (Hughes Clarke, 2016).

154 The first observed type of bathymetric change relates to “delta-lip collapses” - large  
155 ( $>20,000 \text{ m}^3$ ) failures of the delta front. Five such events were observed in 2011;  
156 referred to here as delta-lip collapses A to E (Figures 3 & 4).

157 The second type of bathymetric change relates to upstream migration of channel  
158 bedforms (‘bedform events’). Based on analogies with laboratory experiments,  
159 supported by recent water column imaging, bedform migration is inferred to result from  
160 turbidity currents that generate cyclic steps (Hughes Clarke et al., 2012b, 2014; Hughes  
161 Clarke, 2016; Symons et al., 2016). As event timing can only be constrained to the  
162 nearest ~24 hours, the minimum recurrence interval that can be resolved is one day for  
163 MBES observations. The precise temporal resolution may vary between ~20 and 30  
164 hours, depending on when a particular feature (e.g. delta lip) was surveyed on  
165 successive days. A total of 106 discrete bedform events were identified from the MBES  
166 data, with 49 in the north, 29 in the central and 28 in the south channel (Figure 3). We  
167 sub-divide these ‘bedform events’ based on the morphology at their upslope limit. Some  
168 bedform events include smaller-scale failures near the delta-lip (‘bedform events with  
169 headscars’), but others start mid-slope (typically at ~20 m water depth) without an  
170 obvious landslide scar (‘bedform events without headscars’; Figure 2D&E). We also  
171 classify the amount of vertical change related to each bedform event. Clearly noticeable  
172 change of  $>0.5 \text{ m}$  is significantly above the resolution of MBES and is termed “major”  
173 change. “Minor” change is defined as  $<0.5 \text{ m}$  vertical difference.



174

175 **Figure 2: (A) Squamish prodelta situated within the Upper Howe Sound, British**  
 176 **Columbia showing extent of detailed bathymetry (yellow box) analysed in this**  
 177 **paper. (B) Annotated aerial photograph showing location of delta-top channel. (C)**  
 178 **Location of northern, central and southern channels at Squamish prodelta. ADCP**  
 179 **location is yellow star at outflow of northern channel. Extent of Figure 4 shown by**

180 **yellow box; Difference maps of prodelta illustrating large delta lip failure in**  
181 **northern channel (D) and bedform event in southern channel without a headscar**  
182 **(E). (F) Perspective view of delta-top channel modified from Pratomo (2016).**

183

### 184 **3.3 Direct monitoring of turbidity currents using an ADCP**

185 An upward-looking 600 kHz ADCP was installed for 147 days downstream of the  
186 northern channel (Figure 2C). This ADCP recorded the arrival of turbidity currents to  
187 within 30 seconds. Deployment was continuous from 29/03/11 to 23/08/11 (Julian Day  
188 088-235), with the exception of a 20 day period from 30/6/11 to 20/07/11 (JD181-201)  
189 when the ADCP was buried by the run-out from a major delta-lip failure event. MBES  
190 repeat surveys defined 49 bedform events relating to turbidity currents that caused  
191 morphological change in the northern channel. However, only 22 turbidity currents  
192 were recorded at the more distal ADCP location (Figure 3). At the ADCP location, flow  
193 speeds were recorded in the region of 0.3 to 1.5 m/s, with thicknesses from 10 m to 40  
194 m, with some lasting for over one hour. Material suspended by turbidity currents took  
195 more than 8 hours to settle out (Hughes Clarke et al., 2012b).

196 The variables considered as causes here include tides, river discharge and earthquakes.  
197 Hourly tidal measurements in metres relative to mean sea level were used (Hughes  
198 Clarke et al., 2012). Hourly river discharge data, recorded in m<sup>3</sup>/s, from September 2010  
199 to November 2011 were obtained 12 km upstream at Brackendale, Environmental  
200 Canada station 08GA022. The timing and magnitude of earthquake events are from the  
201 Earthquakes Canada database ([http://earthquakescanada.nrcan.gc.ca/stndon/NEDB-](http://earthquakescanada.nrcan.gc.ca/stndon/NEDB-BNDS/bull-eng.php)  
202 [BNDS/bull-eng.php](http://earthquakescanada.nrcan.gc.ca/stndon/NEDB-BNDS/bull-eng.php)). In some locations worldwide, turbidity currents coincide with  
203 larger wave heights (Xu et al., 2004). However, because the Squamish Delta has limited

204 fetch it experiences small wave heights (Stronach et al., 2006), and consequently wave  
205 height is excluded from this analysis. Non-parametric statistical tests (Mann-Whitney  
206 and Kolmogorov Smirnov) are used to determine whether specific conditions (river  
207 discharge and tidal state) correlate with the *timing* of a turbidity current, or if they  
208 cannot be discerned from a scenario in which turbidity currents are randomly triggered.  
209 Generalised Linear and Proportional Hazard Models (Clare et al., 2016 and references  
210 therein; Appendix A) then test for the significance of the same variables on the *rate* at  
211 which turbidity currents occur.

## 212 **4. Results**

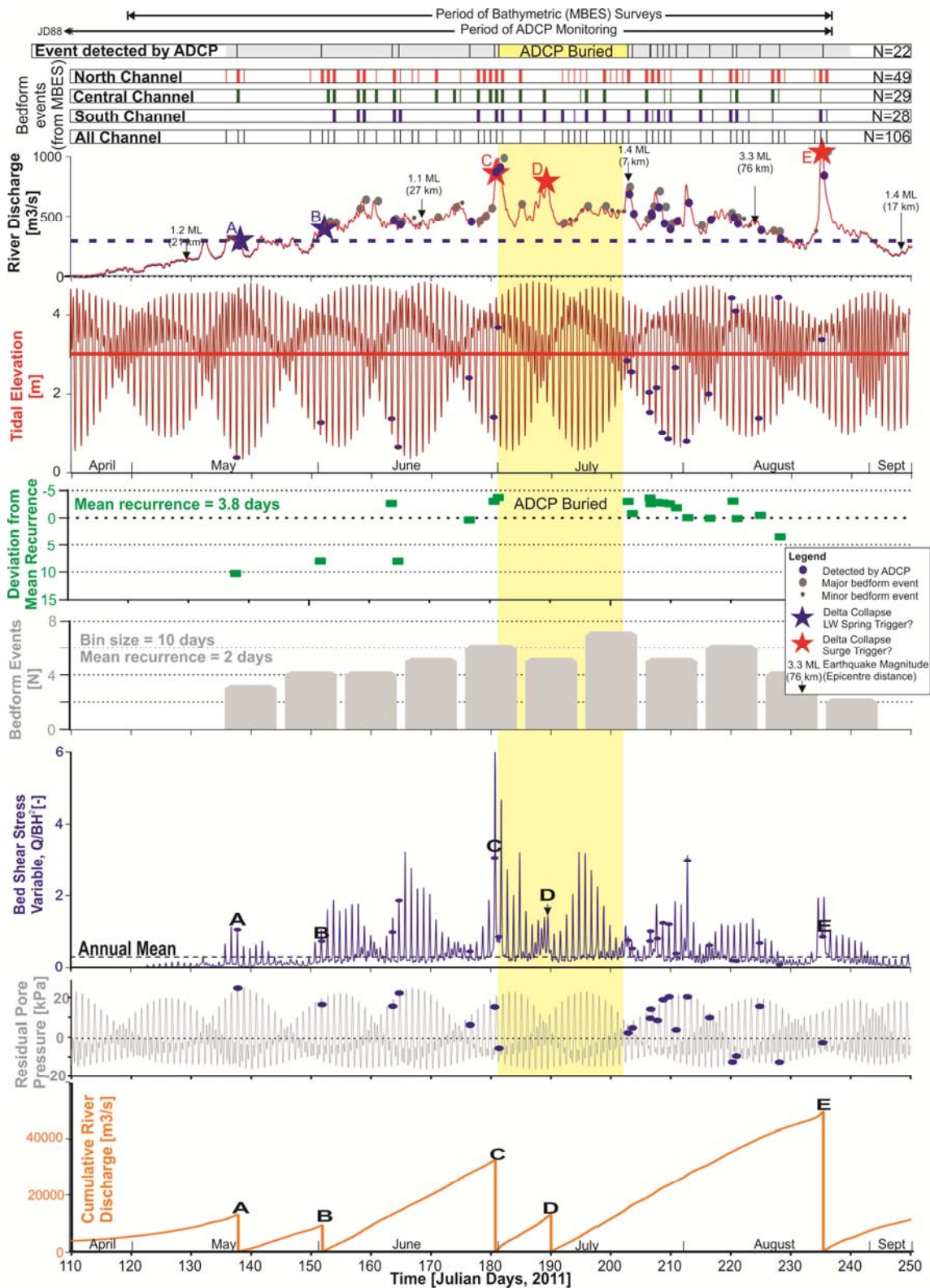
### 213 **4.1. Delta-lip collapses**

214 Slope instability typically arises under one or more conditions that can include i) over-  
215 steepening of the slope through differential deposition; ii) loading of the upper slope by  
216 sediment; iii) removal of sediment from the toe of the slope; and iv) changes in pore  
217 pressure regime (Bromhead, 2006). The latter can be caused by rapid sedimentation  
218 (where insufficient time exists to allow dissipation of excess pore pressures), the  
219 presence of gas in pore spaces otherwise filled with water, and transient perturbations  
220 such as cyclic storm wave loading, earthquake activity, and hydraulic fluctuations due  
221 to the tidal cycle. The rate of pore pressure dissipation is governed by the diffusion  
222 pathway distance (thickness of overburden) and the coefficient of consolidation ( $c_v$ ),  
223 which is in turn a function of permeability and sediment compressibility (Terzaghi  
224 1943). Here we investigate how such processes may have preconditioned and triggered  
225 large collapses of the delta-lip.

226 Delta-lip collapses A, B, C and E occurred at the head of the Northern Channel, while D  
227 was at the head of the Central Channel (Figure 4). On each of the days within which a  
228 delta-lip collapse was determined from MBES surveying at the head of the Northern  
229 Channel, we also detect a turbidity current at the ADCP location. We assume that these  
230 particular turbidity currents were directly related to run-out from the delta-lip collapse  
231 and not to an initial hyperpycnal flow. River concentrations were too low for  
232 hyperpycnal flow conditions (Hughes Clarke et al., 2014) and the presence of large  
233 scars on the delta lip (Figure 4) support this assumption. We thus use the more precisely  
234 constrained ADCP monitoring to determine the timing of delta lip failures A, B, C and  
235 E. As delta-lip collapse D occurred at the head of the Central Channel, and during the  
236 period under which the ADCP had been buried, it is not possible to provide a more  
237 precise timing for that specific event.

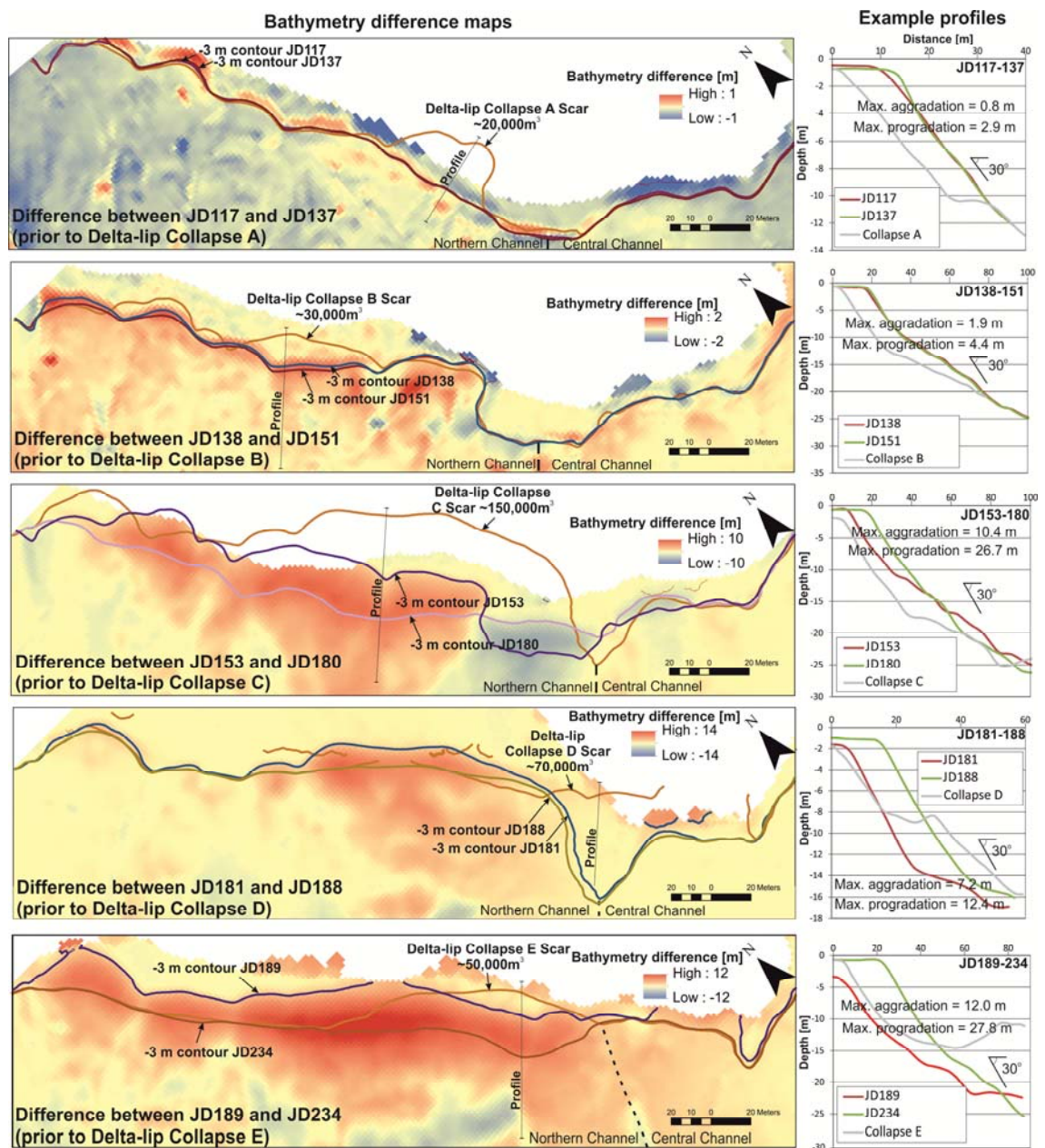
238 The first two major delta-lip collapses we detected (A and B) coincided with relatively  
239 low spring tides (0.25 and 0.69 m respectively), but not peaks in river discharge  
240 (Figures 3 & 6; Hughes Clarke et al., 2012a). Subsequent delta-lip collapses (C, D and  
241 E) occurred shortly (8-11 hours) after the three largest river discharge peaks ( $>775$   
242  $\text{m}^3/\text{s}$ ). The largest delta-lip collapse (C), that buried the ADCP, occurred  $\sim 8$  hours ( $\pm$   
243  $\sim 15$  minutes) after the second highest recorded river discharge. While there are  
244 differences in the instantaneous discharge for these events, the cumulative river  
245 discharge prior to failure is above a minimum threshold ( $>90,000 \text{ m}^3/\text{s}$ ) for all delta-lip  
246 collapses (Figure 3). Difference maps show the accumulation of sediment at the delta-  
247 lip (Figure 4). Sediment accumulation at the delta-lip, prior to each lip failure (presented  
248 as maximum vertical aggradation/seaward progradation) was: 0.8 m/2.9 m (A), 1.9  
249 m/4.4 m (B), 10.4 m/26.7 m (C), 7.2 m/12.4 m (D), 12.0 m/27.8 m (E). Based on  
250 sediments sampled from the Fraser River delta slope, dissipation of excess pore

251 pressures due to the additional sediment deposited prior to delta-lip collapses C, D and  
252 E would have taken weeks to months (Figure 5). The mean grain size for the Fraser  
253 River prodelta slope is c. 0.25 mm (Chillarige et al., 1997) compared to 0.5-0.8 mm for  
254 the Squamish delta top, and 0.1-0.2 mm for the Squamish prodelta slope (as measured  
255 from grab samples), so that analogy is not entirely unreasonable. However, Fraser River  
256 sediments feature a higher proportion of fine sediments than Squamish which would  
257 promote longer pore pressure dissipation times. The presence of gas hosted in pores will  
258 also inhibit dissipation (Figure 5). Squamish delta slope sediments host considerable  
259 amounts of gas (Hughes Clarke et al., 2012b), but precise quantities are not known at  
260 this time. Hence, some degree of uncertainty exists on the exact time for excess pore  
261 pressure dissipation. The smaller loads applied prior to delta-lip collapses A and B may  
262 have been less significant, but the tidal-induced pore pressure effects may have been  
263 more pronounced for these events in May and early June.  
264



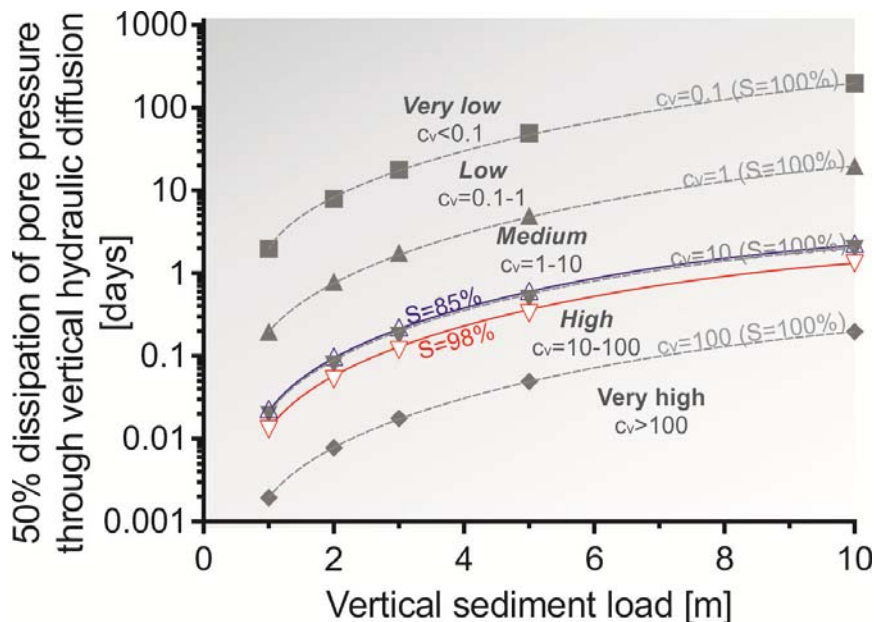
265  
 266 **Figure 3 (previous page): Time series of event occurrence and variables discussed**  
 267 **in this paper. Top four staves show timing of turbidity currents recorded by ADCP**  
 268 **and bedform events detected from MBES (thicker bars denote major [ $>0.5$  m]**

269 change; thinner bars denote minor [ $<0.5$  m] change), river discharge and  
 270 earthquakes, tidal elevation, recurrence of turbidity currents detected at ADCP  
 271 location, bedform event frequency per 10 day bins, delta-top bed shear stress  
 272 variable, residual pore pressure at 10 m below seafloor, and cumulative river  
 273 discharge leading up to delta-lip collapses A to E (annotated).  
 274



275

276 **Figure 4: Bathymetry difference maps (left panels) for time periods building up to**  
 277 **a delta-lip collapse. River flow is from the top. Location of maps is shown in Figure**  
 278 **2C. Changes in bathymetric depths are shown for time period between the day of a**  
 279 **delta-lip failure and the day before the next delta-lip failure. Hot colours (red)**  
 280 **illustrate higher net sediment accumulation. Cool colours (blue) illustrate net**  
 281 **sediment loss. Colour scales differ on each panel. The approximate position of the**  
 282 **delta-lip is shown by lines denoting the -3 m water depth contour at the start and**  
 283 **end of each period. Also shown is the extent of the failure scar for each delta-lip**  
 284 **collapse. The division between the Northern and Central Channels is depicted by**  
 285 **dotted line, and only Delta-lip Failure D (JD189) did not occur at the head of the**  
 286 **Northern Channel. Example bathymetric profiles (right panels) are presented for**  
 287 **the start (red) and end (green) of each period, as well as the profile that resulted**  
 288 **from each delta-lip failure event (grey).**



289  
 290 **Figure 5: Time required for 50% dissipation of excess pore pressures following**  
 291 **instantaneous sediment loading of variable thickness. The time to dissipate pore**  
 292 **pressures is highly dependent on the consolidation (or hydraulic diffusivity)**

293 coefficient ( $c_v$ ,  $m^2/year$ ) and the degree of pore fluid saturation (S), where  $S=98\%$   
294 equates to 2% gas saturation. Hollow symbols based on values from Fraser River  
295 for different gas saturations ( $S=85\%$  and  $98\%$ ) (Chillarige et al., 1997). Filled  
296 symbols illustrate sensitivity of dissipation times for the full range of consolidation  
297 rates defined in Lambe and Whitman (2008). Results based on methods in  
298 Terzaghi (1943).

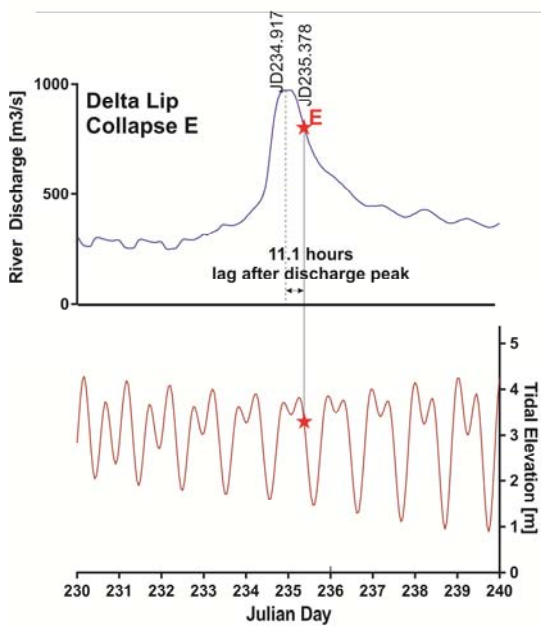
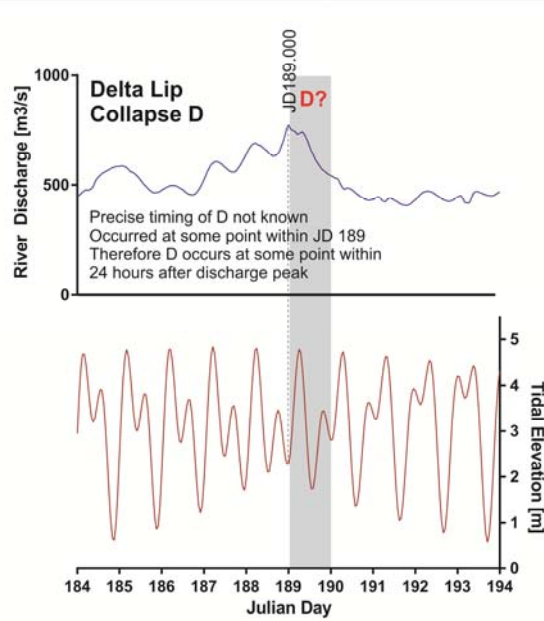
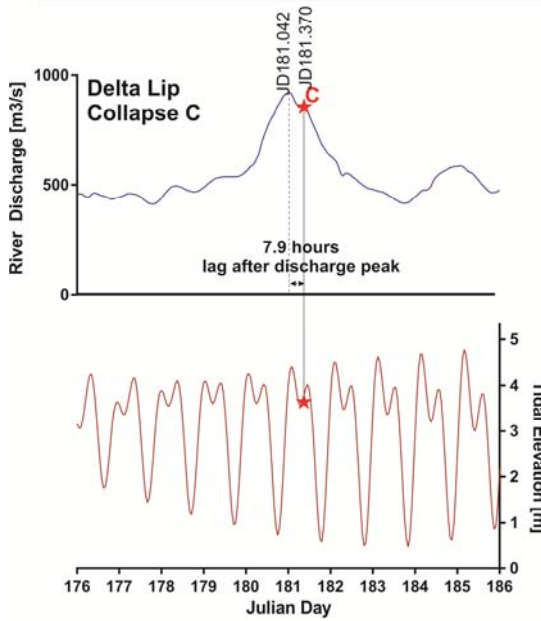
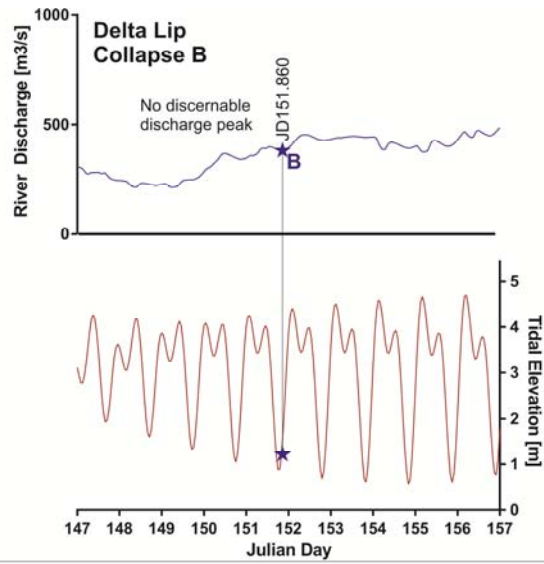
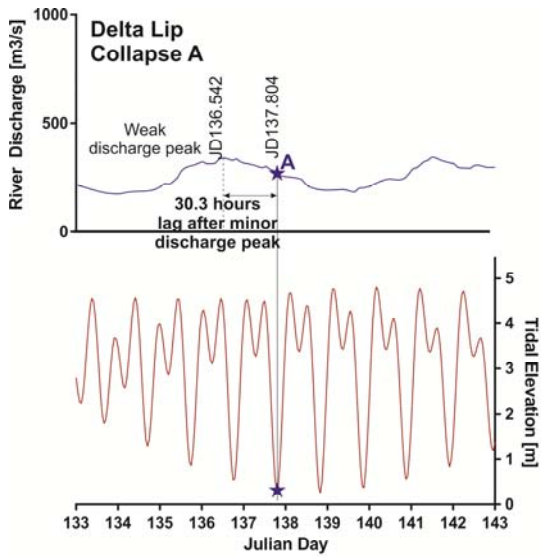
#### 299 4.2. Triggering of events during river floods – via hyperpycnal flow or slope 300 failure?

301 Previous work has suggested that plunging river floodwater may trigger turbidity  
302 currents (Forel, 1888; Mulder et al., 2003), but Hughes Clarke et al. (2014) has shown  
303 that the density threshold required for hyperpycnal flow is not achieved at Squamish for  
304 the discharges seen here. ADCP data shows that delta-lip collapses (C and E) occurred  
305 ~8 to 11 hours after the peak in river discharge (Figure 6). Delays cannot be determined  
306 for delta-lip collapse D as the ADCP was temporarily buried. The peak in river  
307 discharge should also equate to the peak in sediment transport from the river, as the  
308 suspended sediment concentration for Squamish River is higher on the rising limb of a  
309 flood (Hickin, 1989). Based on conservative river velocities of 1 to 3 m/s measured near  
310 and downstream from the discharge monitoring station during a flood peak (Hickin,  
311 1989), it is calculated that river discharge would reach the delta-lip within 1 to 3 hours.  
312 This analysis also assumed that submarine flows took ~30 minutes to travel from the  
313 delta-lip to the ADCP mooring at a speed of 1 m/s which is consistent with that  
314 measured by the ADCP (Hughes Clarke et al., 2012b). The observed lag of 8 to 11  
315 hours post-discharge peak is therefore not explained by the potential maximum lag of  
316 3.5 hours for discharge to reach the ADCP. Delta-lip failure therefore post-dates the

317 peak of flood discharge by several hours. Furthermore, headscarps seen in MBES data  
318 show clearly that the initiation mechanism for events C, D and E was slope failure,  
319 rather than plunging hyperpycnal river discharge (Figure 4; Hughes Clarke et al., 2014).

320

321 **Figure 6 (next page): Time series of river discharge and tidal elevation during**  
322 **delta lip failure events A to E. Timing of delta-lip failures is based on**  
323 **measurements from the ADCP at the end of the Northern Channel. As delta-lip**  
324 **failure D occurred at the top of the Central Channel, and during a time at which**  
325 **the ADCP was buried, the precise timing of delta lip collapse D could not be**  
326 **identified. A major event was noted from the MBES data during JD189; hence**  
327 **event D occurred at some point after a river discharge peak at JD189.0. Therefore**  
328 **it can be inferred there was some time lag, albeit unquantified. River discharge**  
329 **measured at a station 12 km upstream.**



331 **4.3. Did earthquakes trigger delta-lip collapses or turbidity currents?**

332 Only one earthquake of  $>2 M_L$  occurred during the monitoring period (76 km to the  
333 south-east,  $3.3 M_L$  on JD 224.25), but it did not coincide with any turbidity current or  
334 delta-lip collapse events. Two  $<2 M_L$  earthquakes occurred within 30 km of Squamish  
335 in the same period, one of which preceded an event observed on the ADCP by  $\sim 8$  hours,  
336 and the other by  $\sim 8$  days (Figure 3). Therefore, small  $<3.3 M_L$  earthquakes did not  
337 trigger slope failures or turbidity currents, during the 2011 monitoring period. The  
338 influence of larger earthquakes or series of small earthquakes cannot be determined  
339 because neither occurred during the monitoring period.

340 **4.4. Does river discharge control the ‘switch on’ and recurrence rate of**  
341 **turbidity currents?**

342 We now discuss the triggering of bedform events that are not associated with large  
343 delta-lip failures. Only the first of the bedform events occurred when river discharge  
344 was below the annual average discharge ( $253 \text{ m}^3/\text{s}$ ). This first bedform event did,  
345 however, occur 24 hours after a discharge peak of  $342 \text{ m}^3/\text{s}$ . More than three quarters of  
346 bedform events occurred when river discharge was  $>75\%$  of its annual range (Figure 7);  
347 which is a highly significant difference ( $p < 0.0001$ ) for *event timing* (Table 1).

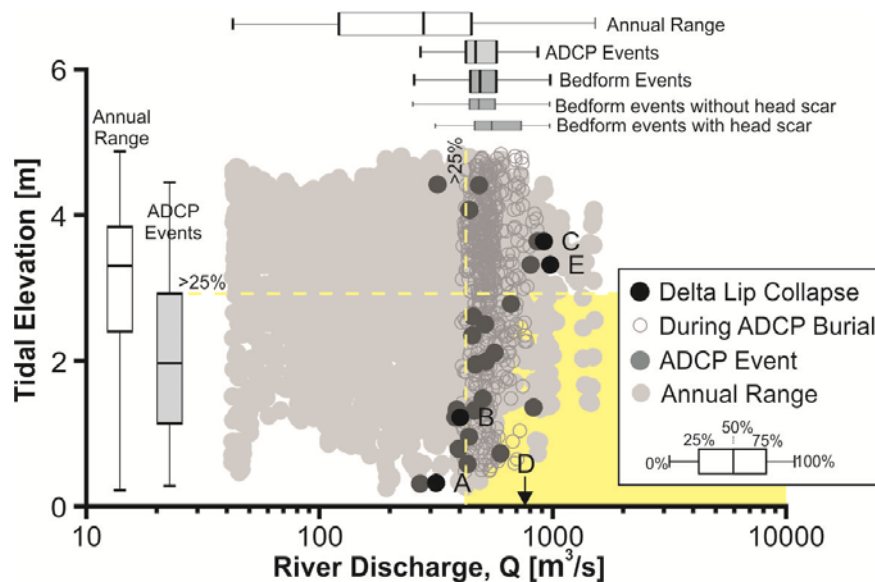
348

349 **Table 1: Results of non-parametric statistical tests to determine significance of**  
 350 **difference between annual range in variables against the range coincident with**  
 351 **events detected by the ADCP. Bold italicised values are significantly different**  
 352 **( $p < 0.05$ ).**

353

Test Type		River Discharge	Tidal Elevation	Residual Pore Pressure
Kolmogorov-Smirnov	p-value	<i><b>0.0005</b></i>	<i><b>&lt;0.0001</b></i>	<i><b>0.0017</b></i>
	Kolmogorov-Smirnov D	0.4330	0.5492	0.4021
Mann-Whitney	p-value	<i><b>&lt;0.0001</b></i>	<i><b>0.0002</b></i>	<i><b>0.0005</b></i>
	Mann-Whitney U	25918	30300	32070
	Difference: Actual	186.7	-1.320	12.12
	Difference: Hodges-Lehmann	221.1	-1.110	8.929
	95% Confidence Interval	140.1 to 301.3	-1.630 to -0.055	9.09 to 19.39

354



355

356 **Figure 7: Comparison of background annual variations in tidal elevation and river**  
 357 **discharge with those at the time of observed turbidity currents detected by the**  
 358 **ADCP. Box and whiskers demonstrate the range of conditions, where whiskers**

359 cover the full range of data and boxes show 25<sup>th</sup>, 50<sup>th</sup> and 75<sup>th</sup> percentiles. Dark  
360 grey solid circles are conditions at the time of turbidity currents detected by the  
361 ADCP. Black solid circles are conditions at delta-lip collapses. Light grey solid  
362 circles are conditions during which no events were observed. Hollow circles  
363 indicate the period during which the ADCP was buried, and hence it is not known  
364 if any events occurred or not. As the ADCP was buried during delta-lip collapse D,  
365 only the approximate river discharge can be quantified (arrow on x axis). Yellow  
366 fill indicates range of conditions within which 75% of events occurred.

367 The general trend of increasing river discharge towards the freshet peak in June and July  
368 is mirrored by more frequent turbidity current activity (Figure 3). The number of  
369 bedform events detected per 10 day bin was more than double (1 event every 1.43 days)  
370 than at the start (1 event every 3.33 days) of the freshet (Figure 3). The frequency of  
371 turbidity currents directly detected by the ADCP also increased, particularly between  
372 JD180-225 (1 event/3.8 days). River discharge is also shown to be a strongly significant  
373 variable on event *recurrence rate*. Both Proportional Hazard (p=0.002-0.0008) and  
374 Generalised Linear Models (p=0.002-0.003) indicate that river discharge is highly  
375 significant in relation to flow recurrence rate.

#### 376 **4.5. Do delta-lip collapses and turbidity currents coincide with low tides?**

377 Two major delta-lip collapses (A and B) correspond to relatively lower river discharge  
378 conditions compared with the rest of the freshet (<480 m<sup>3</sup>/s). These events occurred  
379 during relatively low minimum spring tides; 2.8 m and 1.9 m below the mean annual  
380 tidal elevation for the A and B delta-lip collapses respectively (Figure 3). While the  
381 three other delta-lip collapse events correspond to extreme river discharges, they also  
382 correspond to tidal elevations that are lower than 75% of the annual conditions (Figure

383 7). The tidal elevation at the initiation time of turbidity currents unrelated to delta-lip  
384 collapses is also significantly different to that of the annual range (Figure 3), and is  
385 unlikely to be due to random chance (Mann-Whitney test,  $p=0.0002$ ; Kolmogorov-  
386 Smirnov test,  $p=0.0005$ ; Table 1).

387 Tidal loading may cause shallow slope failure by liquefaction (Kramer, 1988).  
388 However, this process cannot explain the largest delta-lip collapses, due to the depth of  
389 their failure surface ( $>10$  m). Changes in subsurface pore-water pressure due to tidal  
390 drawdown are probably more important – particularly in gas-saturated sediments.  
391 Squamish Prodelta sediments are known to be gas saturated (Hughes Clarke et al.,  
392 2012a). Pore-water pressure response is calculated at 10 m below seafloor based on the  
393 method in Chillarige et al. (1997), which was developed for a similar site at the Fraser  
394 River Delta, British Columbia (full method is presented in Appendix A; Figure 3).  
395 Similarly to the tidal analysis, pore pressures during the events are found to be  
396 significantly different to those for the annual range ( $p=0.0005-0.0017$ ), with most  
397 events occurring at times featuring positive residual pore pressures (i.e. coincident with  
398 lowered hydrostatic pressure).

#### 399 **4.6. Does turbidity current timing relate to a combination of tide and river** 400 **discharge effects?**

401 The next step is to relate river discharge and tidal elevation in a simple manner to bed  
402 shear stress, and hence the rate at which bedload drives sediment over the delta-lip. Bed  
403 shear stress controls rates of bedload transport by the river to the delta-lip, and hence  
404 rates of sediment deposition and lip migration (Pratomo, 2016). Here, a bed shear stress  
405 variable,  $Q/BH^2$ , is derived at the delta-lip, where  $Q$  is river discharge, and  $B$  and  $H$  are  
406 the delta-top channel width and height respectively (Appendix A). A rectangular

407 channel is assumed, so that  $H$  changes in response to tidal fluctuations, but  $B$  remains  
408 constant. Thus, the output is conservative because if a U- or V-shaped channel was  
409 considered, the channel width,  $B$ , would be considerably narrower during lowered tides;  
410 providing a much higher value for the bed shear stress. The Generalised Linear Model  
411 and Proportional Hazards Model analyses do not indicate any degree of significance  
412 ( $p>0.89$ ) for this bed shear stress variable in relation to the *rate* at which flows recur.  
413 However, the significance of bed shear stress in relation to the *specific timing* of  
414 individual flows is considerably greater than just considering tidal elevation or river  
415 discharge in isolation (Mann-Whitney,  $p\ll 0.0001$ ; Kolmogorov-Smirnov test,  
416  $p\ll 0.0001$ ; Table 1). More than 75% of the events seen by the ADCP correspond to the  
417 upper 25% of the annual range of the dimensionless bed shear stress variable (Figure 3).  
418 Thus, bed shear stress may govern the instantaneous triggering of an individual flow,  
419 but not the rate at which they recur.

## 420 **5. Discussion**

421 We now discuss the results of the statistical analysis in relation to flow and failure  
422 triggering and conditioning. In Table 2 we summarise and compare our findings with  
423 the existing hypotheses proposed for slope failure and mass flow triggering at offshore  
424 river deltas.

### 425 **5.1. Extreme river flood discharge leads to delta-lip collapses not hyperpycnal** 426 **flows**

427 Suspended sediment concentrations are unlikely to be high enough to generate dense,  
428 plunging hyperpycnal flow from direct river discharge at the Squamish Prodelta and  
429 other rivers in the fjords of British Columbia (Bornhold et al., 1994; Mulder and

430 Syvitski, 1995; Hill et al., 2008). Extreme peaks in river discharge, with suspended  
431 sediment concentrations of  $<1 \text{ kg/m}^3$  (Syvitski et al., 1987), did not trigger hyperpycnal  
432 flows, rather they correspond with large ( $>20,000 \text{ m}^3$ ) delta-lip failures a few hours after  
433 the flood peak (Figure 6). If the ADCP data were used in isolation, a hyperpycnal flow  
434 may have been interpreted as the initiating process from a broad correspondence in  
435 timing. This important observation is only possible due to the repeated MBES surveys  
436 which identified the occurrence of delta-lip failures. This type of MBES data is typically  
437 not available, and it illustrates a need for caution in assuming that submarine flows that  
438 occur during river floods are solely triggered by plunging hyperpycnal flood-water.

439 During periods of extreme discharge the river delivers sediment to the delta top and lip,  
440 but it does not immediately trigger turbidity currents on the offshore delta slope.  
441 Instead, sediment rapidly builds up to prograde the delta-lip over a period of hours, prior  
442 to a delta-lip collapse.

443 Hughes Clarke et al. (2014) noted that wholesale plunging of river water was not  
444 possible, but did image sediment settling downwards from a surface plume using water  
445 column echo-sounders. It is inferred that convective fingering is responsible for this  
446 settling, which can occur at densities of  $<1 \text{ kg/m}^3$  (Yu et al., 2000; Parsons et al., 2001).  
447 Optical backscatter measurements, coupled with conductivity, temperature and density  
448 (CTD) profiling, indicate that the upper parts of some turbidity currents are less dense  
449 than the surrounding water (Hughes Clarke et al., 2014). This density contrast may be  
450 explained by freshwater becoming entrained by sediment that settles out from the river  
451 discharge plume. As the mixture crosses the pycnocline, the sediment settles out and  
452 may start to flow downslope under its excess density. In the later stages of the flow, as  
453 sediment drops out due to deceleration, the entrained freshwater becomes net buoyant as  
454 it is less dense than the lowermost sediment-rich layer and also the overlying seawater;

455 it therefore lofts (Sparks et al., 1993). The lower-most (<2 m) part of the flow, which is  
456 presumably where the majority of sediment is transported, is not imaged by the optical  
457 backscatter measurements (Hughes Clarke et al., 2014). This mechanism of sediment  
458 settling may be important for the triggering of flows that are not associated with an  
459 obvious failure scarp (Hughes Clarke et al., 2014).

## 460 **5.2. Conditioning and triggering of delta-lip collapses**

461 The triggering of delta-lip collapses relates to a combination of factors, but a seismic  
462 trigger with magnitude  $M_L < 3.3$  can be ruled out for the time interval studied (Figure  
463 3). The cumulative effects of both river discharge and tidal drawdown are shown to  
464 precondition and trigger delta-lip failures (Figure 8). We suggest that two different  
465 triggering mechanisms operate, depending on the sediment supply provided by the river.  
466 Hence these mechanisms may provide insights into the triggers of slope failures at  
467 deltas both with both low and high rates of sediment supply. In the early part of the  
468 freshet (prior to mid-June), the background river discharge is low, and hence so is the  
469 sediment discharge (Hickin, 1989). Moderate progradation (<5 m) and vertical loading  
470 (<2 m) of the delta-lip may initiate preconditioning to failure, but the influence of  
471 extreme low spring tides appears to be the dominant control on generating transient  
472 excess pore pressures that provide the near-instantaneous trigger (Figure 8). However,  
473 once the river bedload increases in the freshet-peak (mid-June to August), sediment  
474 delivery causes major cumulative progradation (up to 30 m) and vertical loading (up to  
475 12 m) at the delta-lip. Pore pressures do not have time to dissipate under such loading,  
476 and are raised further following sudden sediment delivery at river flood peaks.  
477 Following these peaks, there is a lag of 8-12 hours, after which a delayed delta-lip  
478 collapses occurs independent of tidal elevation (Figure 8). Our analysis assumes

479 effective vertical drainage pathways for pore pressure dissipation, and hence  
480 homogeneous permeability. However, preconditioning for delayed failures may also be  
481 in part due to the presence and geometry of relatively lower permeability layers, below  
482 which pore pressures can build up through time (Özener et al., 2009). Such delayed  
483 slope failures may be common, particularly at the offshore deltas of high discharge  
484 rivers, but have rarely been recognized because of the lack of temporally well-  
485 constrained data. However, a series of sequential seafloor cable breaks in the Gaoping  
486 submarine canyon offshore Taiwan occurred three days after a major peak in river  
487 discharge related to Typhoon Morakot (Carter et al., 2014). The breaks occurred under  
488 normal river discharge conditions; hence, it is interpreted that a delayed failure occurred  
489 leading to remobilization of sediment that had rapidly accumulated at the peak in river  
490 discharge (Carter et al., 2014).

491         The spatial distribution of the five delta-lip collapses also appears to be important  
492 in determining the temporal sequence of their occurrence (Figure 4). Delta-lip collapse  
493 A occurred near the most seaward extent of the delta lip following progradation due to  
494 sediment build up. Removal of failed sediment oversteepened its western flank, where  
495 delta-lip collapse B occurred 14 days later. Sediment continued to build up on the delta-  
496 lip, until the post-failure morphology was no longer visible. The extent of the next  
497 collapse, C at JD181 corresponded to the first major peak in river discharge. It covered  
498 areas that failed during lip-collapses A and B. This may indicate that loose sediment,  
499 rapidly-deposited over the previous failure scars, was more susceptible to failure. Eight  
500 days later, delta-lip collapse D occurred at the seaward extent of the delta-lip which  
501 adjoined the eastern flank of collapse C's headscarp. The final collapse, E, occurred 46  
502 days later, also at the most seaward extent of the delta-lip. It covering a similar area to

503 collapse C; which was also an area of loose, recently deposited sediments that may have  
504 been more prone to fail.

### 505 **5.3. River discharge is the primary conditioner for turbidity current activity**

506 River discharge is identified as a strongly significant individual variable in relation to  
507 both turbidity current timing and recurrence rate. The Proportional Hazards Model for  
508 the ADCP-observed flows indicate the rate at which turbidity currents occur increases  
509 by 0.6% (+/-0.4%; 95% confidence intervals) for every 1 m<sup>3</sup>/s increase in river  
510 discharge. This only holds for conditions where the river discharge exceeds a minimum  
511 threshold – defined here as the mean annual river discharge (~253 m<sup>3</sup>/s).

### 512 **5.4. Tidal effects amplify the effects of river discharge to trigger turbidity** 513 **currents**

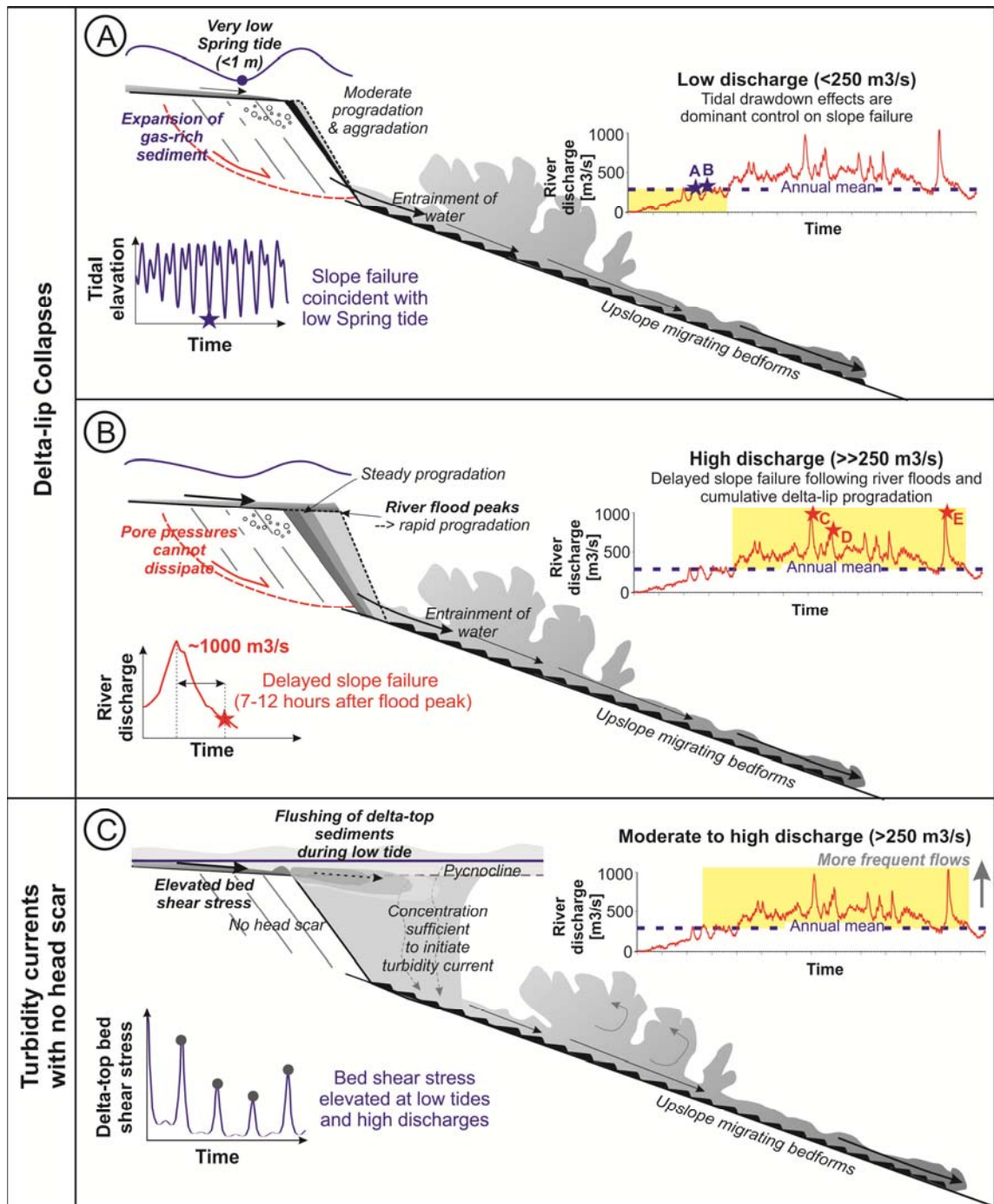
514 Lowered tides are shown to have a significant relationship with turbidity current timing,  
515 albeit less significant than river discharge. This is presumably because sediment supply  
516 from the river is the main control on turbidity current frequency. We suggest that tidal  
517 effects may enhance the effects of river discharge in two ways. In the first, additive or  
518 sequential effects are significant, such that the slope is preconditioned by increased  
519 sediment load and tidal influence (e.g. pore pressure change). This addition of two  
520 effects then tips the balance to trigger a failure. The second scenario is related to  
521 amplified effects, where combinations of low tides and elevated river discharge enhance  
522 bed shear stresses, causing erosion and increased flux of bedload driven over the delta  
523 lip. Given the low river discharge early in the season, the contribution of lower tides is  
524 likely to be the more important factor. Only a relatively small amount of shear stress is  
525 necessary at the start of the freshet to flush the mouth bar accumulated over the winter.

526 The significance of tidal effects will reduce as river discharge increases throughout the  
527 freshet, amplifying bed shear stresses and increasing the likelihood of seaward flushing  
528 of delta-top sediments. This flushing, coupled with the near-constant settling of  
529 convective fingers of sediment, then triggers flows on the upper prodelta slope. This  
530 mechanism is thus distinct from a hyperpycnal flow trigger and does not require a slope  
531 failure that forms a headscarp. This mechanism may explain why a damaging turbidity  
532 current occurred on the Fraser River delta-slope, yet no headscarp was identified  
533 (Lintern et al., 2016). The flow was capable of displacing a one tonne seafloor  
534 observatory and severed an armoured cable.

## 535 **6. Conclusions**

536 Here we analyse the first field data that provides the timings of > 100 failure and  
537 turbidity currents, from Squamish Prodelta. The largest peaks in river discharge did not  
538 result in hyperpycnal flows, rather they caused more rapid progradation of the delta  
539 front, which ultimately led to large delayed delta-lip collapses (>20,000 m<sup>3</sup>/s).  
540 Sedimentation on the delta-top and progradation of the delta-lip appear to precondition  
541 the slope to failure. The ultimate trigger is then either due to exacerbation of pore  
542 pressures on the slope via tidal drawdown effects, or rapid sedimentation during river  
543 floods. As suggested qualitatively by Hughes Clarke et al. (2012), elevated river  
544 discharge is now quantitatively demonstrated to be a primary control for the 'switch on'  
545 of turbidity current activity. River discharge is a statistically significant variable in  
546 explaining the frequency at which turbidity currents occur. Each 1 m<sup>3</sup>/s increase in  
547 discharge above the threshold discharge (mean annual level) corresponds to a 0.6%  
548 increase in flow likelihood. Below that level the system is 'switched off'. Tidal  
549 elevation also contributed to the timing of turbidity currents. This is most likely due to

550 amplification of the effect of river discharge causing elevated bed shear stresses on the  
 551 delta-lip, and seaward flushing of delta-top sediments.



552

553 **Figure 8: Illustration of mechanisms inferred to be responsible for triggering of**  
 554 **delta-lip collapses. (A and B) Events associated with headscars, triggered during**  
 555 **low rates of delta-lip progradation (A) and high rates of progradation (B). (C)**  
 556 **Events which are not associated with headscars and thus slope failure, nor with**  
 557 **hyperpycnal river discharge.**

<b>Control</b>	<b>Trigger Mechanism (<i>cross-referenced to Figure 1</i>)</b>	<b>Nature of failures/flows</b>	<b>Reference</b>	<b>Evidence at Squamish prodelta as a trigger?</b>
River Discharge	Direct plunging of river water as hyperpycnal flow (1).	Near-continuous flows coincident with peak of flood event.	Mulder and Syvitski (1995); Mulder et al. (2003); Bornhold et al. (1994).	Not a trigger for the largest flows, which are triggered by failures. Sediment concentrations too low in river.
	Localised mixing of the freshwater-saline interface causes enhanced settling of sediment due to convective fingers (2).	Episodic flows coincident with periods of enhanced settling from a surface plume.	Parsons et al. (2001); Hughes Clarke et al. (2014, Hughes Clarke, 2016).	Possible trigger, but not for the largest flows, which are triggered by failures.
	Delta failure: Sediments reside temporarily on parts of the delta slope to be later remobilised as they become more unstable (3).	Turbidity currents following main flood event.	Bornhold et al. (1994); Hughes Clarke et al. (2012a, 2014).	Yes.
	Elevated river discharge enhance bed shear stresses, causing erosion and increased flux of bedload driven over the delta lip (9). Can be exaggerated during low tides.	River discharge sweeps accumulated coarse-grained bar and channel sediments (with any bedload) directly onto the steep delta front slopes.	Prior and Bornhold (1989); Bornhold et al. (1994).	Yes.
	Grain avalanches: Bedload swept offshore may avalanche down steeply-inclined foresets on Gilbert-type delta (10).	Sediment accelerates down inclined foresets and transitions into a turbidity current.	Gilbert (1885); Postma et al. (1988).	Possible trigger.
Tides	Excess pore pressures in low permeability materials during low tides triggers liquefaction (4).	Transient pore pressure changes cause liquefaction which leads to slope instability (unlikely to have any effect >1 m below seafloor).	Johns et al. (1986); Chillarige et al (1997).	No, because failure occurs too deep (> 10m) in sediment.
	Tidal drawdown on gaseous sediments causes expansion and slope failure (5).	Reduction in effective stress during lowered tides where gas can be brought out of solution to trigger deep-seated failure.	Christian et al. (1997); Chillarige et al. (1997); Hughes Clarke et al. (2012a, 2014).	Possible trigger, but not for all failures.
	Lowered tide constricts delta-top channel and enhances bed shear stresses, causing erosion and increased flux of bedload driven over the delta lip (9). Can be exaggerated during high river discharges.	Constriction of channel leads to elevated bed shear stresses causing erosion, and deposition on delta-lip or triggering of sediment avalanches.	Prior and Bornhold (1989); Hughes Clarke et al. (2012a, 2014; Hughes Clarke, 2016).	Possible trigger for flows as sediment is flushed offshore.
Storm Waves	Cyclic loading of delta-lip sediments induces slope failure (7).	Transient pore pressure changes cause liquefaction.	Prior et al. (1989).	No.
Upper to mid-prodelta processes	Localised liquefaction or breaching within submarine channels or incision of steep margins by previous flow (8).	Triggers turbidity current on prodelta slope.	Van Den Berg et al. (2002); Mastbergen and Van Den Berg (2003).	Possible trigger for many major and minor bedform events that do not have obvious failure scarps.
Earthquakes	Strong ground motion and development of transient excess pore pressures (6).	Destabilisation of slope sediments due to shaking, liquefaction or strain softening.	Prior and Bornhold (1989); Bornhold and Prior (1990); Bornhold et al. (1994).	Not a trigger during 2011 surveyed period

558 **Table 2: Natural triggering mechanisms hypothesised for slope failures and flows**  
559 **at offshore river deltas**

560 **Acknowledgments and Data**

561 We thank David Piper, Thomas Hubble, one anonymous reviewer and Editor Martin  
562 Frank for their insightful reviews, which substantially improved the manuscript. We  
563 acknowledge the following grants: NERC International Opportunities Fund  
564 (NE/M017540/1) “Coordinating and pump-priming international efforts for direct  
565 monitoring of active turbidity currents at global test sites”; and NERC Environmental  
566 Risks to Infrastructure Innovation Programme (ERIIP) (NE/N012798/1) “What threat  
567 do turbidity currents and submarine landslides pose to strategic submarine  
568 telecommunications cable infrastructure”. Talling was supported by a NERC and Royal  
569 Society Industry Fellowship hosted by the International Cable Protection Committee  
570 (ICPC). Appendix A (expanded methods) and Appendix B (full statistics results) can be  
571 found in the online supporting material. Animated timelapse bathymetry for the  
572 multibeam surveys on the upper part of the prodelta can be found online at  
573 [http://www.omg.unb.ca/Projects/SQ\\_2011.html/](http://www.omg.unb.ca/Projects/SQ_2011.html/).

574 **References**

- 575 Bhattacharya, J. P., and Giosan, L. (2003). Wave-influenced deltas: Geomorphological  
576 implications for facies reconstruction. *Sedimentology*, 50(1), 187-210.
- 577 Bornhold, B. D., and Prior, D. B. (1989). Sediment blocks on the sea floor in British  
578 Columbia fjords. *Geo-marine letters*, 9(3), 135-144.
- 579 Bornhold, B. D., Ren, P., and Prior, D. B. (1994). High-frequency turbidity currents in  
580 British Columbia fjords. *Geo-Marine Letters*, 14(4), 238-243.

581 Bromhead, E. (2006). *The stability of slopes*. CRC Press.

582 Carter, L., Gavey, R., Talling, P., and Liu, J. (2014). Insights into Submarine  
583 Geohazards from Breaks in Subsea Telecommunication Cables. *Oceanography*, doi:  
584 10.5670/oceanog.2014.40.

585 Chillarige, A. V., Morgenstern, N. R., Robertson, P. K., and Christian, H. A. (1997).  
586 Seabed instability due to flow liquefaction in the Fraser River delta. *Canadian*  
587 *Geotechnical Journal*, doi: 10.1139/T97-019.

588 Christian, H. A., Mosher, D. C., Mulder, T., Barrie, J. V., and Courtney, R. C. (1997).  
589 Geomorphology and potential slope instability on the Fraser River delta foreslope,  
590 Vancouver, British Columbia. *Canadian geotechnical journal*, 34(3), 432-446.

591 Clare, M.A., Talling, P.J., Challenor, P., Malgesini, G., and Hunt, J. (2014). Distal  
592 turbidites reveal a common distribution for large (> 0.1 km<sup>3</sup>) submarine landslide  
593 recurrence. *Geology*, G35160-1.

594 Clare, M. A., Talling, P. J., Challenor, P. G., and Hunt, J. E. (2016). Tempo and  
595 Triggering of Large Submarine Landslides: Statistical Analysis for Hazard  
596 Assessment. In *Submarine Mass Movements and their Consequences* (pp. 509-517).  
597 Springer International Publishing.

598 Cooper, C., Wood, J., and Andrieux, O. (2013). Turbidity Current Measurements in the  
599 Congo Canyon. *Proceedings of Offshore Technology Conference*, 1-4 May 2013,  
600 Houston, Texas.

601 Dietrich, P., Ghienne, J. F., Normandeau, A., and Lajeunesse, P. (2016). Up-slope  
602 migrating bedforms in a proglacial sandur delta: Cyclic steps from river-derived  
603 underflows?. *Journal of Sedimentary Research*, doi:10.2110/jsr.2016.4.

- 604 Droxler, A. W., and Schlager, W. (1985). Glacial versus interglacial sedimentation rates  
605 and turbidite frequency in the Bahamas. *Geology*, 13(11), 799-802.
- 606 Forel, F.A. (1888). Le ravin sous-lacustre du Rhône dans le lac Léman. *Bulletin de la*  
607 *Société Vaudoise des Sciences Naturelles*, 23:85-107
- 608 Gilbert, G.K. (1885). The topographic features of lake shores U.S. Geol. Surv., Annu.  
609 Rep., 5, pp. 75–123
- 610 Hickin, E. J. (1989). Contemporary Squamish River sediment flux to Howe Sound,  
611 British Columbia. *Canadian Journal of Earth Sciences*, 26(10), 1953-1963.
- 612 Hill, P. R., Conway, K., Lintern, D. G., Meulé, S., Picard, K., and Barrie, J. V. (2008).  
613 Sedimentary processes and sediment dispersal in the southern Strait of Georgia, BC,  
614 Canada. *Marine environmental research*, 66, S39-S48.
- 615 Hughes Clarke, J.E. (2016). First wide-angle view of channelized turbidity currents  
616 linking migrating cyclic steps to flow characteristics. *Nature Communications*.  
617 doi:10.1038/ncomms11896
- 618 Hughes Clarke, J. E., Brucker, S., Muggah, J., Church, I., Cartwright, D., Kuus, P. and  
619 Eisan, B. (2012a). The Squamish Prodelta, monitoring active landslides and turbidity  
620 currents. *Canadian Hydrographic Conference*.
- 621 Hughes Clarke, J. E., Marques, C. V., and Pratomo, D. (2012b). Imaging active mass  
622 wasting on a fjord delta, Squamish, British Columbia. In *Submarine Mass Movements*  
623 *and their Consequences*, V. Springer International Publishing.
- 624 Hughes Clarke, J. E., Marques, C. R. V., and Pratomo, D. (2014). Imaging active mass-  
625 wasting and sediment flows on a fjord delta, Squamish, British Columbia. In

626 Submarine Mass Movements and Their Consequences (pp. 249-260). Springer  
627 International Publishing.

628 Ingersoll, R. V., Dickinson, W. R., & Graham, S. A. (2003). Remnant-ocean submarine  
629 fans: largest sedimentary systems on Earth. *Special Papers - Geological Society of*  
630 *America*, 191-208.

631 Johns, M. W., Prior, D. B., Bornhold, B. D., Coleman, J. M., and Bryant, W. R. (1986).  
632 Geotechnical aspects of a submarine slope failure, Kitimat Fjord, British Columbia.  
633 *Marine Georesources and Geotechnology*, 6(3), 243-279.

634 Kramer, S.L. (1988). Triggering liquefaction flow slides in coastal soil deposits,  
635 *Engineering Geology*, 26, 17-31.

636 Lambe, T. W., and Whitman, R. V. (2008). *Soil Mechanics SI version*. John Wiley &  
637 Sons.

638 Lambert, A., and Giovanoli, F. (1988). Records of riverborne turbidity currents and  
639 indications of slope failures in the Rhone delta of Lake Geneva. *Limnology and*  
640 *Oceanography*, 33(3), 458-468.

641 Lintern, D. G., Hill, P. R., and Stacey, C. (2016). Powerful unconfined turbidity current  
642 captured by cabled observatory on the Fraser River delta slope, British Columbia,  
643 Canada. *Sedimentology*.

644 Mastbergen, D. R., and Van Den Berg, J. H. (2003). Breaching in fine sands and the  
645 generation of sustained turbidity currents in submarine canyons. *Sedimentology*, doi:  
646 10.1046/j.1365-3091.2003.00554.

- 647 Mulder, T. and Syvitski, J. P. (1995). Turbidity currents generated at river mouths  
648 during exceptional discharges to the world oceans. *The Journal of Geology*, 285-299.
- 649 Mulder, T., Syvitski, J. P., Migeon, S., Faugeres, J. C., and Savoye, B. (2003). Marine  
650 hyperpycnal flows: initiation, behavior and related deposits. A review. *Marine and*  
651 *Petroleum Geology*, doi:10.1016/j.marpetgeo.2003.01.003
- 652 Orton, G. J., and Reading, H. G. (1993). Variability of deltaic processes in terms of  
653 sediment supply, with particular emphasis on grain size. *Sedimentology*, 40(3), 475-  
654 512.
- 655 Özener, P. T., Özyayın, K., and Berilgen, M. M. (2009). Investigation of liquefaction  
656 and pore water pressure development in layered sands. *Bulletin of Earthquake*  
657 *Engineering*, 7(1), 199-219.
- 658 Parsons, J. D., Bush, J. W., and Syvitski, J. P. (2001). Hyperpycnal plume formation  
659 from riverine outflows with small sediment concentrations. *Sedimentology*, 48(2),  
660 465-478.
- 661 Piper, D. J., and Normark, W. R. (2009). Processes that initiate turbidity currents and  
662 their influence on turbidites: a marine geology perspective. *Journal of Sedimentary*  
663 *Research*, 79(6), 347-362.
- 664 Postma, G., Nemec, W., and Kleinspehn, K. L. (1988). Large floating clasts in  
665 turbidites: a mechanism for their emplacement. *Sedimentary Geology*, 58(1), 47-61.
- 666 Pratomo, D.G. (2016). Coupling of repetitive multibeam surveys and hydrodynamic  
667 modelling to understand bedform migration and delta evolution, PhD Thesis,  
668 University of New Brunswick.

669 Prior, D.B., and Bornhold, B.D. (1989). Submarine sedimentation on a developing  
670 Holocene fan delta. *Sedimentology* 36.6 (1989): 1053-1076.

671 Prior, D. B., Coleman, J. M., and Bornhold, B. D. (1982). Results of a known seafloor  
672 instability event. *Geo-Marine Letters*, 2(3-4), 117-122.

673 Prior, D. B., Bornhold, B. D., Wiseman, W. J., and Lowe, D. R. (1987). Turbidity  
674 current activity in a British Columbia fjord. *Science*, 237(4820), 1330-1333.

675 Prior, D. B., Suhayda, J. N., Lu, N. Z., Bornhold, B. D., Keller, G. H., Wiseman, W. J.,  
676 Wright, L.D., and Yang, Z. S. (1989). Storm wave reactivation of a submarine  
677 landslide. *Nature*, 341(6237), 47-50.

678 Sparks, R.S.J., Bonnecaze, R.T., Huppert, H.E., Lister, J.R., Hallworth, M.A., Mader,  
679 H., and Phillips, J. (1993). Sediment-laden gravity currents with reversing buoyancy.  
680 *Earth and Planetary Science Letters*, 114(2), 243-257.

681 Stronach, J., Zaremba, L., Wong, M., Neil, L. and McLennan, N. (2006). Wave and  
682 current forecast system for the mouth of the Fraser River. Hay and Company  
683 Consultants, Vancouver, 15 pp.

684 Symons, W.O., Sumner, E.J., Talling, P.J., Cartigny, M.J., and Clare, M.A. (2016).  
685 Large-scale sediment waves and scours on the modern seafloor and their implications  
686 for the prevalence of supercritical flows. *Marine Geology*, 371, 130-148.

687 Syvitski, J.P., Burrell, D.C., and Skei, J.M. (1987). *Fjords: processes and products*.  
688 Springer Science & Business Media.

689 Syvitski, J. P. and Shaw, J. (1995). *Sedimentology and geomorphology of fjords*.  
690 *Developments in sedimentology*, 53, 113-178.

691 Talling, P. J., Allin, J., Armitage, D. A., Arnott, R. W., Cartigny, M. J., Clare, M. A., et  
692 al. (2015). Key future directions for research on turbidity currents and their deposits.  
693 *Journal of Sedimentary Research*, 85(2), 153-169.

694 Terzaghi, K. (1943) *Theoretical Soil Mechanics*, John Wiley and Sons, New York,  
695 510 p.

696 Van Den Berg, J. H., Van Gelder, A., and Mastbergen, D. R. (2002). The importance of  
697 breaching as a mechanism of subaqueous slope failure in fine sand. *Sedimentology*,  
698 49(1), 81-95.

699 Wright, L. D. (1977). *Sediment transport and deposition at river mouths: a synthesis*.  
700 *Geological Society of America Bulletin*, 88(6), 857-868.

701 Xu, J. P., Noble, M. A., and Rosenfeld, L. K. (2004). In-situ measurements of velocity  
702 structure within turbidity currents. *Geophysical Research Letters*, 31(9).

703 Xu, J. P., Sequeiros, O. E., and Noble, M. A. (2014). Sediment concentrations, flow  
704 conditions, and downstream evolution of two turbidity currents, Monterey Canyon,  
705 USA. *Deep Sea Research Part I: Oceanographic Research Papers*, 89, 11-34.

706 Yu, W. S., Lee, H. Y., and Hsu, S. M. (2000). Experiments on deposition behavior of  
707 fine sediment in a reservoir. *Journal of Hydraulic Engineering*, 126(12), 912-920.